REGULAR PAPER

The Focused Electrode Ring for Electrohydrodynamic Jet and Printing on Insulated Substrate

Zeshan Abbas[1] · Dazhi Wang[1,2,4] · Liangkun Lu[1] · Zhaoliang Du[1] · Xiangyu Zhao[1] · Kuipeng Zhao[1] · Meng Si[3] · Penghe Yin[1,2] · Xi Zhang[1,2] · Yan Cui[1,2] · Junsheng Liang[1,2]

Abstract

Drop-on-demand electrohydrodynamic jet (DoD E-Jet) printing is considered a well-known type of fabrication method contemporary since it can be used to print high-resolution microstructures (< 1 μm) on various insulating substrates. This paper presents a numerical study of DoD E-Jet printing using a novel combination of needle and focused electrode ring to print stable and consistent microdroplets on a Polyethylene terephthalate substrate. Primarily, a phase field method was used to generate a stable cone-jet morphology that can allow the production of high-resolution micron/nano structures on PET substrates. The numerical simulation of cone-jet morphology was performed by COMSOL multiphysics software. Further, the impact of key parameters such as flow rate and dc positive pulse voltage was studied on cone-jet morphology through numerical simulation. Subsequently, optimized operating parameters i.e., $f = 5.3 \times 10^{-15}$ m^3 s^{-1}, $V_n = 1.9$ kV and $V_r = 0.7$ kV were achieved by performing a series of numerical experiments. Then, optimized parameters by simulation were directly used to print arrays of stable droplets on PET substrate using the focused electrode ring in different locations by regulating distance 0.2 mm to 1.3 mm between needles to focused electrode ring. The minimum size of stable microdrop was measured 3 μm on PET substrate (thickness = 0.2 mm) using a 50 μm size quartz capillary maintaining a distance of 0.2 mm between combined needle and focused electrode ring. The experimental results proved that the simulation model is useful for printing different microstructures on insulating substrates and creating a promising production path for micro-electro mechanical system and nano-electro mechanical system (MEMS and NEMS).

Keywords Phase field method · DoD E-Jet printing · Microdroplets · Focused electrode ring · PET substrate

1 Introduction

In recent years, the demand for MEMS/NEMS devices [1] (i.e., airbag sensors, microphones, projection screen chips, actuators, blood pressure and tire sensors, optical switches and many other products) has grown in consumer and industrial products [2]. MEMS devices consist of gadgets with sizes between 1 and 100 μm and MEMS devices usually vary in size from 10 μm to 1 mm. Moreover, microscale components which are arranged in many string structures that can be in size more than 1000 mm^2 such as digital micro-mirror devices [3]. Microsystem technology (MST) is a method that allows the fabrication of electronic circuits on insulating substrates (i.e., PET) because the role of insulating substrate in power electronics is to provide interconnections to form a printed circuit board and to cooled ingredients. The advanced MST is also applied to print stable microstructures on polyimide films (PI) and glass substrates which are used

✉ Dazhi Wang
d.wang@dlut.edu.cn

1 Key Laboratory for Micro/Nano Technology and System of Liaoning Province, Dalian University of Technology, Dalian 116024, China

2 Key Laboratory for Precision and Non-Traditional Machining Technology of Ministry of Education, Dalian University of Technology, Dalian 116024, China

3 School of Optoelectronic Engineering and Instrumentation Science, Dalian University of Technology, Dalian 116024, China

4 Ningbo Institute of Dalian University of Technology, Ningbo 315000, China

in various electronic devices [4]. The fabrication of MEMS devices evolved from manufacturing process technology in semiconductor device fabrication, i.e. basic techniques are deposition of material layers. Similarly, MEMS devices are composed of silicon, polymers, metals and ceramics materials [5].

The most distinctive substrates used in MEMS devices are polymeric materials such as PET because the polymers are produced in large volumes, with a great variety of material characteristics [6]. MEMS devices can be made from insulating substrates by applying various techniques such as inkjet printing, stereolithography and E-Jet printing. PET substrates have several advantages over rigid glass substrates, such as reduced weight, ease of storage in rolled form [7]. Equally, PET substrates are commonly considered as a highly insulating material in electronics industry and provide thermal insulation on space blankets. However, still PET substrate is facing some critical challenges such as not being able to be used as a direct electrode during DoD and direct writing printing of different microstructures. The stability of a cone-jet morphology and droplets generation have been significantly impaired due to its non-conductive properties [8].

Inkjet printing [9] is the most common printing method in MEMS devices, in which two different techniques are used (i.e., thermal bubbles and piezoelectric forces) to deposit liquid on a substrate to pattern different microstructures [10]. Unlike DoD inkjet printing, the DoD E-Jet printing is a continuous process through which a stream of microscale/nanoscale droplets is created by applying an electrostatic charge between needle and an insulating substrate. Therefore, recently the production of different micron/nano structures using DoD E-Jet printing technology has raised very wide and productive interest, due to its broad applications in MEMS devices [11]. Thus, DoD E-Jet printing technique has many advantages over the stereolithography and inkjet printing methods, such as it provides a three-dimensional structuring, multi-spatial-selective modeling, high resource distribution efficiency, high speed, affordable cost and a non-contact method [12]. As with a single microdroplets stream, the characteristics of individual droplet can be easily varied by changing the flight time, which allows the creation of films with different microstructures during DoD E-Jet printing. In addition, a much smaller droplet can be produced than the needle diameter during the DoD E-Jet printing method. This is due to the high effect of electrostatic forces produced by the applied voltage which overcome the surface tension force and push the functional ink towards the substrate surface [13]. This technology works more efficiently under the simplest needle structure than other complicated types [14]. During, DoD E-Jet atomization, the charged liquid is pull out from the needle when concentration of liquid molecules is greater than needle size at phase field interface

[15]. Therefore, DoD E-Jet printing process has a significant impact on improving the resolution of microdroplets by patterning microstructures on insulating substrates. The method is considered to be the most effective tool in micro and nanofabrication [16] for MEMS devices.

To date, DoD E-Jet printing on different insulating substrates similar to what we are presenting in this existing work has been reported in many research studies around globe. Kim et al. performed experimental study and produced DoD E-Jet patterning in pulsed cone-jet mode at different frequencies. Using the pulse voltage frequency of 25 Hz, the droplets diameter was measured at approximately 95 µm on the substrate surface [17]. Similarly, Abbas et al. performed a numerical simulation of DoD E-Jet and printed different microstructures on PET substrate. The study determined the optimized parameters for the development of DoD E-Jet to print control and stable microstructures on a PET substrate [4]. In another study, Abbas et al. introduced a numerical simulation of the stable cone-jet formation [8] and printed continuous line structures on flexible PET substrate. The study offered 2-phase-field method to optimize parameters for stable cone-jet morphology on a PET substrate using a set of copper control electrodes. Choi et al. proposed experimental study on DoD printing of conductive ink by electrostatic field induced inkjet head. Conductive silver ink was used to aim of printing microstructures and further examined the characteristics of droplets and lines patterned on a PET substrate [13]. Hakiai et al. investigated electrostatic droplet ejection event using planar needle inkjet head [18]. Rahman et al. conducted DoD E-Jet printing with fine resolution of conductive silver traces on the glass substrate. The minimum droplet diameter of 3.6 µm was achieved on the insulating substrate after the sintering process [19]. Li et al. discussed the formation and droplet size of E-Jet drippings mode induced by overlap of an electric pulse at background voltage. The influence of the applied voltage was investigated on the droplet size [20]. Rahman et al. presented a numerical simulation study based on CFD method and investigated the phenomena by generating drops through a nozzle with the help of electrostatic forces [21]. Rahman et al. reported a study of DoD E-Jet printing phenomena by applying the multi-step pulse voltage and patterned minimum droplet diameter of approximately 40 µm at 325 Hz frequency on the glass substrate [22]. Lim et al. proposed a numerical simulation of cone-jet formation in DoD E-Jet atomization using ring electrode. The study was based on CFD model and to generate monodisperse droplets on a substrate surface [23]. To the best of our knowledge and the cited literature, use of a dc pulse voltage at needle and focused electrode rings can cause development in DoD E-Jet process to printing on insulating substrates, but challenges of residual charges still remained. Thus, such a novel geometric model has been explored and introduced by assembling the

focused electrode ring together with the combined needle system during DoD E-Jet printing on PET substrate.

To summarize, we present a numerical simulation study and printing microstructures based on the DoD E-Jet printing method. The study introduces a novel focused electrode ring coupled with the combined needle system. The production-oriented technique was defined in the phase field method in which the resolution, size and stability of microdroplets were consistently improved on a PET substrate. In our previous simulation work, an attempt was made to control the size of a cone-jet morphology and printed microstructures using different size and shape control electrodes around the combined needle. However, to develop stable cone-jet shape and print high-resolution droplets with minimum size on a PET substrate, this new approach overcomes challenges and distortions between the meniscus profiles. Thus, the particular size and shape of a focused electrode ring was chosen using specific values of dc positive pulse voltage and flow rate, which creates a significant effect on the output size of microdroplets. Therefore, the optimized parameters developed by simulation model print stable microdroplets and reduce the reverse impact of residual charges on insulating substrate. Hence, it can play a very important role for patterning on different MEMS devices using DoD E-Jet printing technique.

2 Simulation Model and Experimental Set Up

2.1 Physical Materials

The simulation and experimental studies are based on DoD E-Jet printing method and a typical curing functional ink of UF 3808 is regulated smoothly in a combination needle. The insulating substrate (i.e., PET) is used for printing because PET in its natural state is a colorless and semi-crystalline resin. Depending on how it is processed, PET can be semi-rigid to rigid and is very lightweight. The physical properties of functional ink (Henkel Corporations Group Ltd, United States) were achieved by the suppliers. However, this material can provide excellent mechanical properties for electronic devices, which is widely used in flexible printed electronics. The PET substrates are widely used in biotechnology and MEMS devices, which has high strength barrier that can resist interference for various characteristics. Stainless steel needles and focused electrode ring were used in the experiments according to simulation study. The focused electrode ring was fixed between the steel needle and a substrate using special retaining support. The PET substrate thickness was used 0.5 mm and 0.2 mm in the simulation model as well as in experiments. Table 1 describes the physical properties of functional ink used in phase field simulations for the fabrication of microdroplets.

Table 1 Physcial properties of functional ink UF 3808

Density $(g \cdot cm^{-3})$	Dynamic viscosity (m Pa s)	Surface tension (N/m)	Storage modulus (N/ mm^2)	Dielectric constant
1.16	450,000	0.031	260	3.24

2.2 Governing Equations for Fluid Flow

The conservation of mass and the Navier–Stokes equations are foundations for the motion of functional fluid which is solved in COMSOL multiphysics as explained in Eq. (1). According to E-Jet printing theory, the cone-jet morphology is numerically simulated by using the functional fluid, applied electric field and Cahn–Hilliard equations. The phase field simulation of DoD E-Jet printing process involves tracing the functional liquid–gas interface at needle apex. The schematic diagram of the distribution of forces acting in cone-jet morphology is illustrated in Fig. 1. This numerical work holds two phase fields such as inner liquid and air which were assumed to be immiscible and incompressible.

$$\frac{\delta \rho}{\delta t} \rho \times \nabla \times \vec{u} = 0 \tag{1}$$

where, $\vec{u}$ denotes the flow rate of functional fluid. The multiple forces exerting on the interface of functional fluid was based on the Taylor–Melcher leaky dielectric model [24, 25]. The Navier–Stokes incompressible flow equation is applied in numerical simulation model to solve laminar fluid flow, which is given by Eq. (2).

$$\rho \frac{\partial u}{\partial t} \times (u \times \nabla) \times \vec{u} = \nabla \times \left[-pl + \mu(\nabla \vec{u} + (\nabla \vec{u})^T + F_{st} + F_{es} + \rho g \right] + F \tag{2}$$

where, p is an internal fluid pressure, g is the gravitational acceleration, ρ is a liquid density, while F_{st} and F_{es} represent the surface tension and electric forces, respectively.

$$\frac{\partial \phi_i}{\partial t} - \nabla \times \vec{\mu} \phi_i = \left(\nabla \times \frac{\gamma \lambda}{\sum_T} \right) \times \Delta \psi, \quad \phi = phipf$$
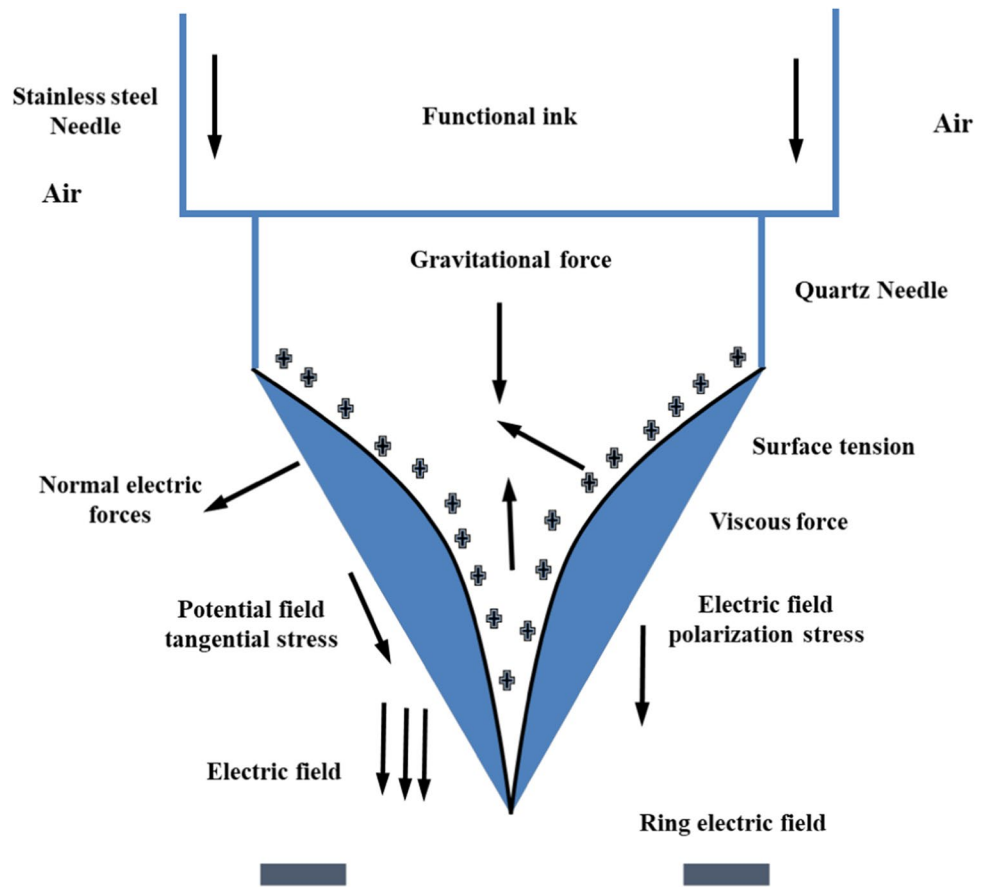$$\lambda = \frac{3 \varepsilon phi \sigma}{\sqrt{8}}, \quad \gamma = X \tag{3}$$

$$\begin{cases} \frac{\partial \phi_i}{\partial t} - \nabla \times \vec{\mu} \phi_i = \left(\nabla \times \frac{M_o}{\sum_T} \right) \times \Delta \eta_i \\ \eta_i = \frac{2 \sum_T}{\theta} \sum_i \prod i \mp j - \left[\frac{1}{\sum_j} (\sigma_i F(\phi) - \sigma_j F(\phi)) \right] \left(\frac{1}{2} - 2\varepsilon c \Delta \theta \psi \right) \end{cases} \tag{4}$$

$$\eta_A = etaA, \quad \eta_B = etaB$$

Therefore, λ is considered real distance between the functional liquids which is used as a variable and in other

Fig. 1 Forces acting around the Taylor cone in DoD E-Jet printing process

words it is known as the determinant coefficient as given in Eq. (3). Where, σ expresses the surface tension. Similarly, σ and ε are executed independently during Cahn Hilliard equations [26]. Thus, $\gamma = X$ indicates the driving force of liquids defined as a variable. The concentration of two liquid phases during numerical simulation is very important to regulate the fluid flow as given in Eq. (4). The Cahn Hilliard potential is an auxiliary variable which is used in the variable contour to assist particle directions during the mass flow of liquids as explained in Eq. (5).

$$F(\phi) = \sigma_{AB}\phi_A^2\phi_B^2 + \sigma_{AC}\phi_A^2\phi_C^2 + \sigma_{BC}\phi_B^2\phi_C^2 + \phi_A\phi_B(\sum_A \phi_A + \sum_B \phi_B)$$

$$\sum_i = \sigma_{i,j} + \sigma_{i,k}$$

(5)

where, The A and B are phase variables used to identify the location of each phase in 2-phase flow model throughout simulation work. So, $\sum_i$ denotes total effect of surface tension. The summation of entire two phases with high concentration values is assumed to be equal to unity in each numerical box as given in the following Eq. (6).

$$\phi_A + \phi_B = 1$$
$$\frac{2}{\sum_i} = \frac{1}{\sum_A} + \frac{1}{\sum_B}$$

(6)

2.3 Governing Equations for Electric Field

Throughout the phase field simulation, the electric field produces effective actuation at the needle outlet. Therefore, electrical forces and surface tension are developed in Navier–Stokes equation [27] as a body forces in simulation model as given in Eq. (7&8).

$$\vec{F}_{es} = q\vec{E} - \frac{1}{2}E^2\nabla\varepsilon + \nabla\varepsilon_0$$

(7)

$$\vec{F}_{st} = -G\nabla\varepsilon\varphi$$

(8)

where, the symbol G is a chemical potential [28] and ϕ demonstrates the phase field symbolic variables. The chemical potential G is categorically given in Eq. (9).

$$G = \lambda\left[-(\nabla^2 \times \varphi) + \frac{\varphi \times (\varphi - 1)}{\theta^2}\right] = \frac{\delta\lambda}{\delta\theta^2}(\psi\varphi)$$

(9)

where, λ is a combination energy density of the fluid, similarly δ is a metal needle width and commonly known as an interface thickness in the simulation model. While calculating the body forces, ε indicates electric permittivity of the functional ink and ε_0 defines permittivity of vacuum. Furthermore, $\nabla\phi$ shows value for gradient of the scalar electric potential. Additionally, (E) expresses electric field near the tip of combined needle system. The Coulomb force is produced when free charges strike down with the interface in presence of ground electrode. The term $(E\varepsilon)$ is a volume charge density in Eq. (10), the electric field is directed by Poisson and volumetric charge density [29] as defined in Eq. (11). Where, $\vec{j}$ is a current density and is demonstrated in Eq. (12).

$$[\nabla \times (\vec{E}\varepsilon)] = \rho_c \tag{10}$$

$$\frac{\delta\rho_c}{\delta t} + \nabla \times \varphi\varphi \times \vec{j} = q \tag{11}$$

$$\rightarrow j = \rho_c u + KE = 0 \tag{12}$$

Thus, K represents the electrical conductivity of functional ink. It also describes the electric current due to charge convection and electric current where charge conduction along the cone profile drives beyond. The phase field simulation begins with the reduction of free external energy. The Cahn–Hilliard equation was generated for two non-miscible fluids over time in simulation models [26, 30], which is given in Eq. (13). To trace a 2-phase interface during laminar phase, the conservative phase-field form was used to determine the interface between liquid phase and gas phase in the simulation model as given in Eq. (14).

$$\frac{\partial c}{\partial t} - \nabla \times (M \times \nabla \times \vec{\mu}) = \nabla \times \frac{\omega\lambda}{\delta^2}\nabla\psi \tag{13}$$

$$\psi = -\frac{3}{2}\sigma\varepsilon\Delta\varphi + 24\frac{\sigma}{\varepsilon}\varphi(1-\varphi)(1-2\varphi) + \left(\frac{\delta^2}{\lambda}\right)\frac{\delta f_{\text{outer}}}{\delta\sigma} \tag{14}$$

where, σ is the surface tension force at interface and μ is a chemical potential of the mixture. Hence, $\frac{\delta f_{\text{outer}}}{\delta\sigma}$ is the gradient of liquid derivative, and M represents as a mobility factor. It is distinguished that the concentration of φ changes in liquid state with a sequence form that has a special value ($\varphi = +1$) and respectively the concentration changes in gaseous state with special value ($\varphi = -1$). Throughout the phase field simulation, phase field variables must satisfy the state $0 \leq \varphi \leq 1$. The physical parameters i.e., σ and ε, are imposed independently during the Cahn–Hilliard potential. To trace the two-phase interface at needle apex using phase field method [31], the functional fluids i.e., liquid and gas are

considered as a single effective unit. The significant fluids properties are demonstrated in Eq. (15).

$$\eta = \eta_g \frac{(1-\varphi)}{2} + \eta_1 \frac{(1+\varphi)}{2} \tag{15}$$

where, η is a fluid real property η_g is the gaseous state property and η_1 is the functional ink property. The dynamic viscosity and relative permittivity of fluids place strong influences on the phase field variables (φ).

2.4 Numerical Simulation

The equations above in governing section describe the viscous motion of a functional fluid, the expression of an electric field in a fluid, the tracking of a two-phase interface, and the coupling of a flow field to the electric field. In this work, the cone-jet morphology is simulated under ternary phase field state. The combined needle system was used in phase field simulation model. It can be seen from Fig. 2 that cone-jet morphology in DoD E-Jet technology involves two basic physics fields, i.e., a flow field and an electric field, and the coupling of the two physics fields. Similarly, amid them flow field contains one liquid phase and one gaseous phase. According to DoD E-Jet Reynolds number, the hydrodynamic field selects the laminar flow module because the working voltage is dc positive pulse voltage [32]. Further, the electrostatic field selects the electric field module where the two independent physical fields are interconnected through multiphysics module. The simulation research focuses on the morphological changes of two-phase interface (the inner liquid-outer air interface) at different time durations. Therefore, the study type is transient. According to the principle of combined needle DoD E-Jet printing process, the operative electric field is distributed in large space between the combined nozzle and ground electrode. This area has three-dimensional axial symmetry and existence of liquid flow is not considered. The three-dimensional electric field can be simplified as a two-dimensional axisymmetric electric field. After the functional fluid is applied then electric field distribution is only affected by flow of liquid near the interface of printing nozzle. Considering that the diameter of cone-jet is much smaller than the inner diameter of printing nozzle in order to clearly observe the formation of microdroplets and reduce the cost of simulation calculation of fluid flow. Therefore, the key simulation area is limited to inner diameter of the nozzle in phase field DoD E-Jet printing nozzle. According to the schematic diagram of phase field simulation scheme as shown in Fig. 3, the electrostatics and laminar phase flow physics were computed in multiphysics contour to generate stable microdroplets on different
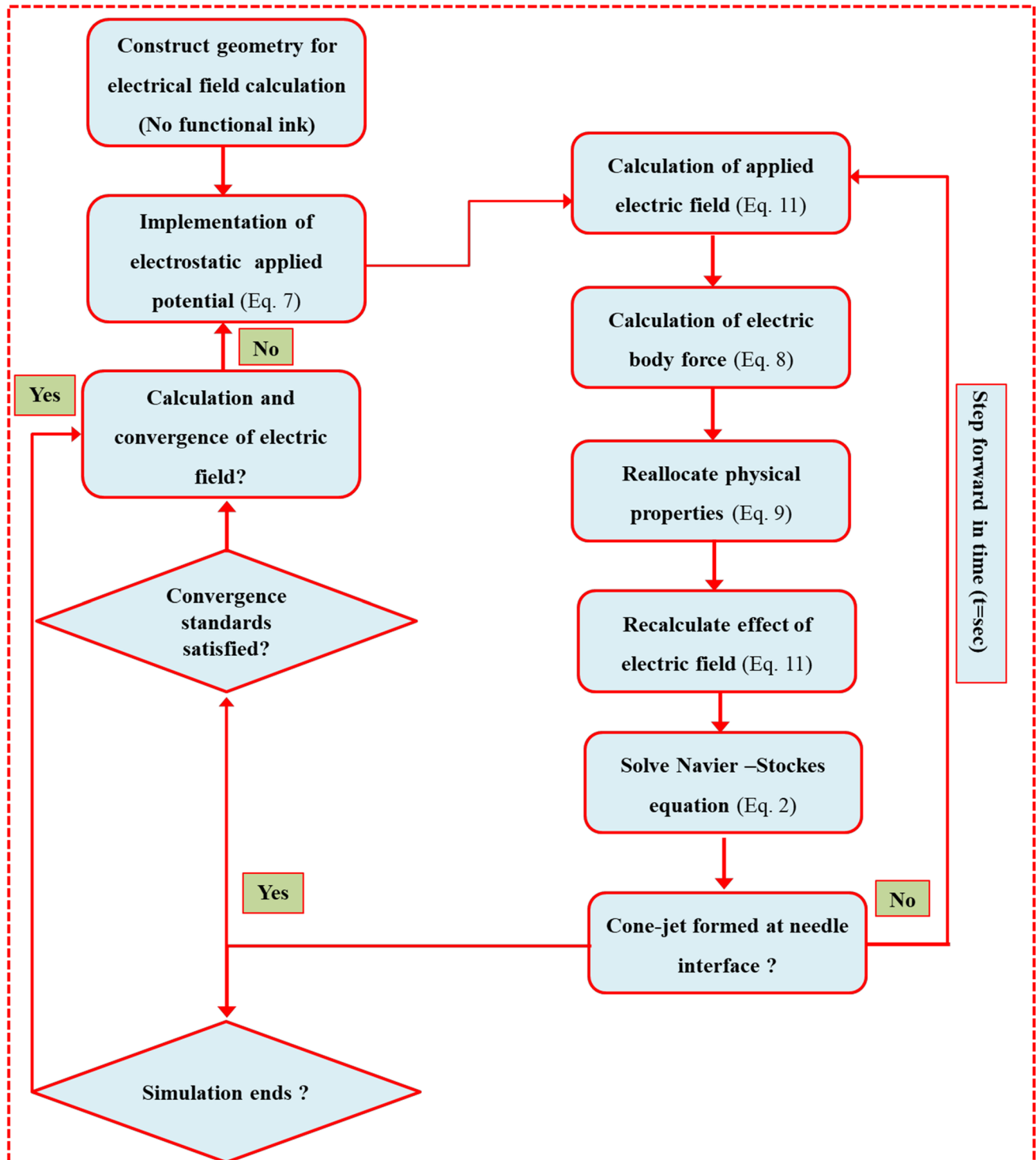
Fig. 2 Flow chart of phase field simulation scheme

insulating substrates. The physics curve and phase field model variables are controlled by time dependent component throughout study period. However, the times are resolved on contour in range of (0, 5e-6, 0.2) with respect to time-dependent solver. In the existing axisymmetric model, the basic geometry and boundary conditions were set as those used by our research team during the numerical simulation for DoD E-Jet printing process [4, 8, 31, 33].
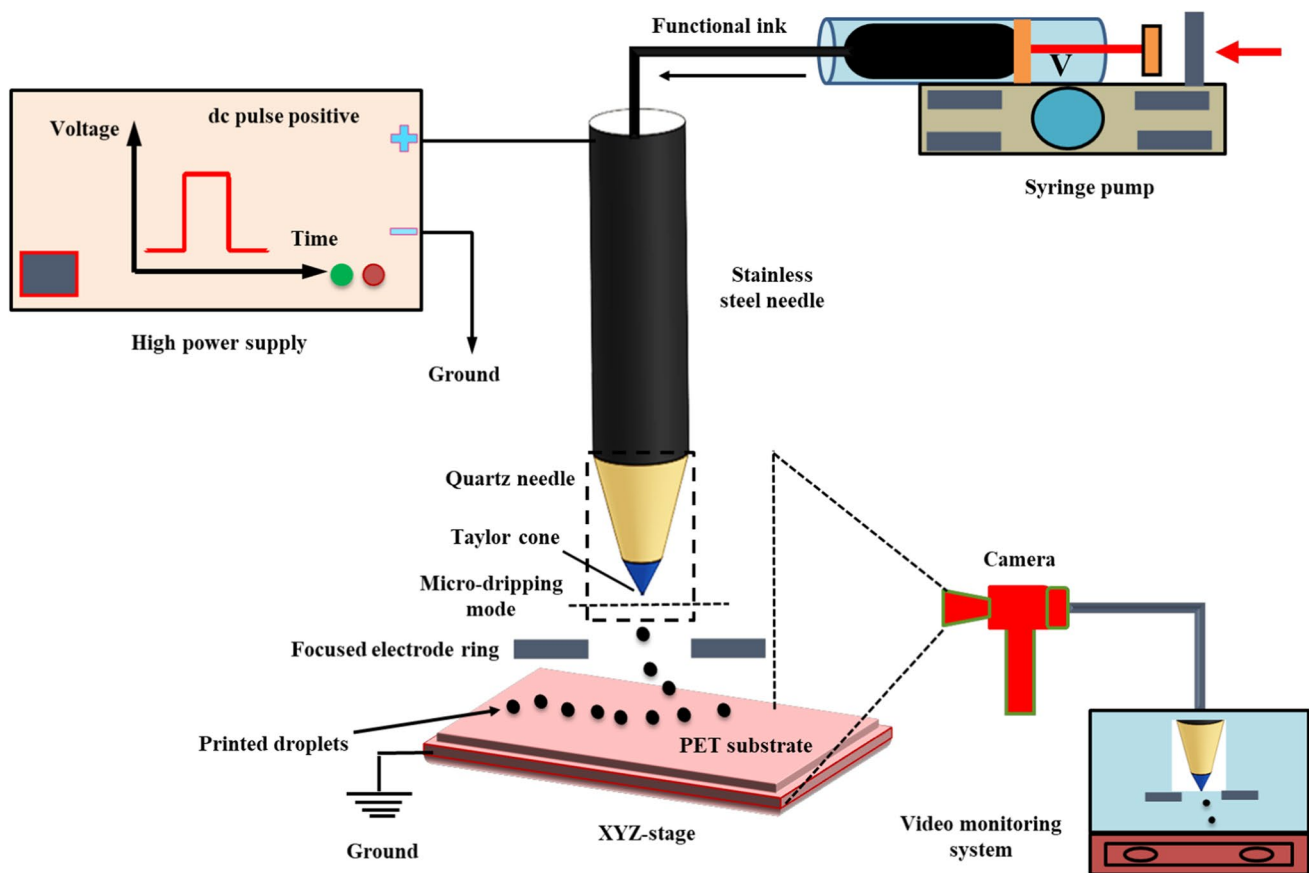
Fig. 3 The schematic diagram of DoD E-Jet printing process

2.4.1 Establishment of Simulation Model and Setting of Boundary Conditions

In order to reduce the amount of calculation and improve the efficiency of simulation model, the three-dimensional structure is simplified to a two-dimensional axisymmetric structure based on axial symmetry of combined needle DoD E-Jet printing process. The numerical simulation model for E-Jet printing, the geometric model and setting of boundary conditions are shown in Fig. 4a. In addition, the finer meshing system for the simulation model was setup in mesh contour as shown in Fig. 4b. Table 2 summarizes the boundary conditions of the electrostatic field and flow field simulation. Further, φ denotes the electric potential of electrostatic field similarly u and P respectively represent the fluid velocity and pressure. Among them, A is the inner liquid inlet, which satisfies $\varphi = V_0$, $u = Q_{inner}/A_{inner}$, where V_0 is the voltage, Q_{inner} is the inner liquid flow rate, and A_{inner} is the effective flow area of inner liquid. More, B is the outer wall of combined needle, which satisfies $\varphi = V_0$, $u = Q_{outer}/B_{outer}$, where Q_{outer} is the flow rate of outer air, and B_{outer} is the effective flow area of outer air near wall side. Thus, C is the wall of focused electrode ring, which satisfies $\varphi = V_0$, $u = 0$. Thus, D is the charge density of

focused electrode ring, which satisfies $\varphi = V_0$, $u = 0$. Moreover, E is the outlet of combined needle structure which satisfies $\varphi = 0$, $P = 0$. So, G is an axisymmetry of the geometric model, which satisfies $\varphi_r = 0$, $u_r = 0$, d_r refers to the radial component of electric potential, and u_r refers to the radial component of velocity. F is a boundary of the entire computational territory which satisfies $\varphi = V$, $P = 0$, and the value of V is not constant and changes with calculation time. The geometric model dimensions simulated in this study are mainly based on commercial needles, in which the inner diameter of a steel needle was kept 365 µm and outer diameter was set to 700 µm. Similarly, inner diameter of quartz capillary was maintained at 50 µm and outer diameter was set to 365 µm, respectively. In addition, to obtain stable cone-jet for fabrication of microdroplets on insulating substrates during DoD E-Jet printing process, the focused electrode ring was used in between steel needle and a PET substrate. The thickness of focused electrode ring was kept at 1 mm, respectively. Similarly, the distance between needle and copper focused electrode ring can be regulated from 0.2 mm to 1.5 mm. The inner diameter of focused electrode ring was set to 3 mm and outer diameter was maintained at 10 mm. In order to reduce the amount of
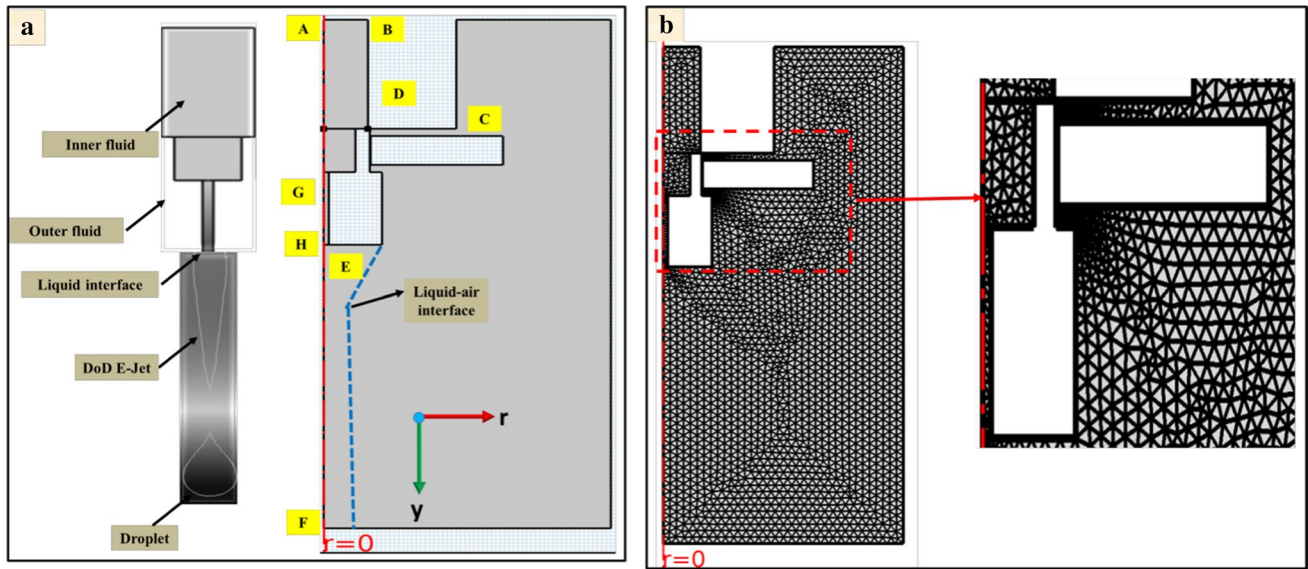
Fig. 4 The numerical simulation model for the DoD E-Jet printing (**a**) Geometric model and setting of boundary conditions (**b**) The finer meshing for the simulation model

Table 2 Simulation boundary conditions of electrostatic field and flow field

Boundary	Electrostatic condition	Hydrodynamic condition
A: Needle inlet	$\varphi \times \vec{j} = V_0$	$u = Q_{\text{inner}}/A_{\text{inner}}$
B: Needle wall	$\varphi = V_0$	$w = 0, u = 0$
C: Focused electrode ring wall	$\varphi = V_0$	$w = 0, u = 0$
D: Focused electrode ring charge	$\varphi = V_0$	$w = 0, u = 0$
E: Needle outlet	$\varphi \times \vec{j} = V_0$	$u = Q_{\text{outer}}/A_{\text{outer}}$
G: Axi-symmetry	$\frac{\mathrm{d}V}{\mathrm{d}r} = 0$	$u = 0, \frac{\mathrm{d}w}{\mathrm{d}r} = 0$
F: Boundary of computational territory	$V = 0$	$p = 0, u = 0$
H: Air territory	$V = 0$	$p = 0, u = 0$

calculation, improve simulation efficiency and accuracy, the simulation model has been simplified in the following aspects.

- Simplifying a three-dimensional model into a two-dimensional axisymmetric model.
- Ignore the outer diameter of the outer needle.

The justification for this is that the needle shape is axisymmetric and two-dimensional axisymmetric model is sufficient to express the combined needle model. Similarly, the simulation difficulty and calculation amount can be greatly simplified and outer diameter of the needle has no influence on flow field.

3 Results and Discussion

3.1 Simulation of DoD E-Jet

The DoD E-Jet printing technology (known electrojet printing) is a new type of micro-nano structure forming method based on electrohydrodynamic effect and inkjet printing technology (thermal bubble type, piezoelectric type) adopts a "push" driving method. The major difference is that, the E-Jet printing uses electric field force to "pull" the liquid to form very thin jet morphology with a
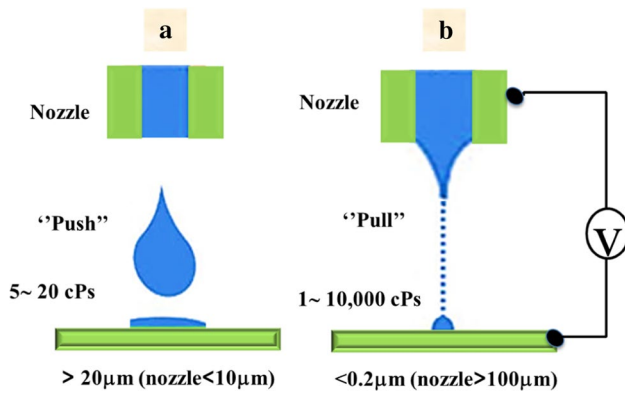
Fig. 5 Schematic diagram of traditional DoD inkjet printing and DoD E-Jet printing [34]

diameter much smaller than inner diameter of the needle. The comparison of two techniques is discussed in the schematic as shown in Fig. 5. The DoD E-Jet printing technology can pattern manufacturing of micron and sub-micron high resolution structures without clogging nozzle and has a very wide range of material applicability such as polymers, ceramics, metals, inorganic functional materials, and biological materials. In addition, E-Jet printing technology has simple process, low cost, no need for molds or masks and no special environmental requirements. This model simulated a stable cone-jet mode which was later transformed into a microdripping mode due to regulation of high pulse voltage on needle and focused electrode ring. The study discusses influence of several parameters on cone-jet and microdroplets size.

3.1.1 Electric Potential Effect on DoD E-Jet Evolution

In the preliminary examination of the effect of working parameters and microdroplets generation on PET substrates, the distribution of electrical potential (V) around the needle tip was evaluated at initial and final intervals, respectively. Since, the electric potential distribution is the most immediate internal factor that forms a DoD E-Jet morphology for stable droplets on substrate surface. As mentioned in Fig. 6a, the light pink color indicates distribution of electric potential around needle interface at initial time interval (0.0184 s). The region around needle tip determines abundance of electric potential which is not rich compared to final time interval. Similarly, Fig. 6b illustrates dark pink color which indicates the distribution of electric potential around needle interface at final time interval (0.0999 s).

Likewise, when the electrical field lines are set impartially charged, then electric potential is evenly distributed at 2-phase interface and gradually it generates cone-jet profile over the volume fraction of liquid. The comparison illustrates that maximum electrical charges are concentrated around top view of Taylor cone with increasing time intervals gradually in the electric potential contour. Lastow et al. determined this electric field lines distribution for cone-jet shape, but the study did not include a droplet break-up model [32]. When electric charges accumulate to a certain degree, the electrical shear force is sufficient to overcome the surface tension. Then, the cone-jet is formed and moves towards the substrate surface. Subsequently, the electric field lines increase charge accumulation near combined needle interface. However, the effect of shear electric force is further increased to overcome the surface tension, and then microdroplets are formed on a PET substrate. The photograph
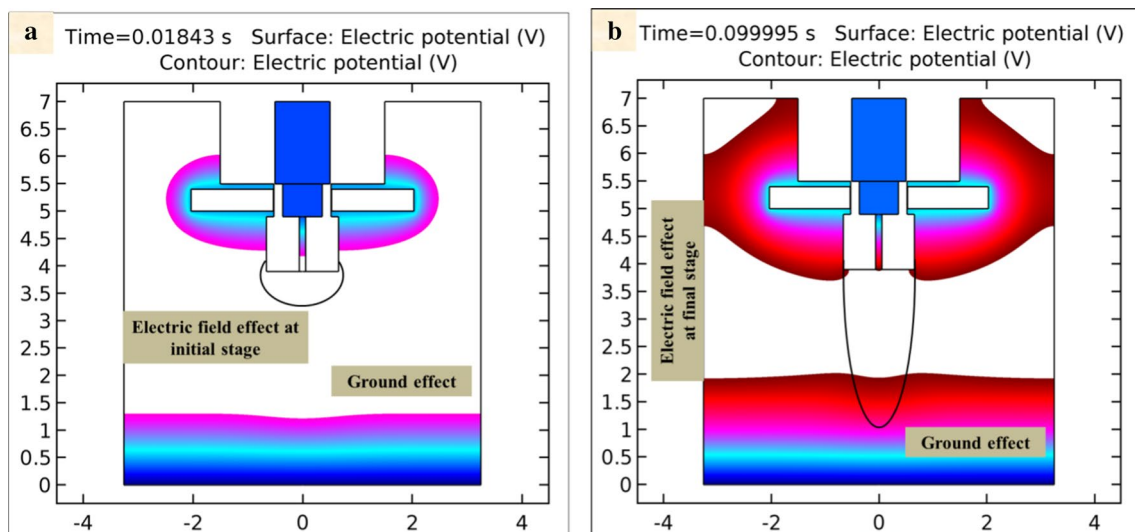

Fig. 6 The distribution of electric potential at different time intervals (**a**) $t = 0.0184$ s (initial) (**b**) $t = 0.0999$ s (final)

of electric potential distribution is taken at optimized value of applied voltage and flow rate i.e., $f = 5.3 \times 10^{-15}$ m^3 s^{-1}, $V_n = 1.9$ kV and $V_r = 0.7$ kV.

3.1.2 Microdroplets Generation Under Different Focused Electrode Ring Locations

The DoD E-Jet printing method is a reasonable fabrication technique for MEMS devices to generate high-resolution and consistent microdroplets on the PET substrate. In order to control microdroplets size and cone-jet morphology, the optimized voltage values are required for specific needle geometry. In this work, we regulate dc positive pulse voltage on both the combined needle system and focused electrode ring. There were a series of experiments performed to obtain optimized parameters using focused electrode ring in different locations. Similarly, Fig. 7 shows the morphological difference of simulated results at different dc positive pulse voltages and flow rates. Where, the applied voltage values vary such as $V_n = 1.5$ kV and 1.9 kV, $V_r = 0.3$ kV and
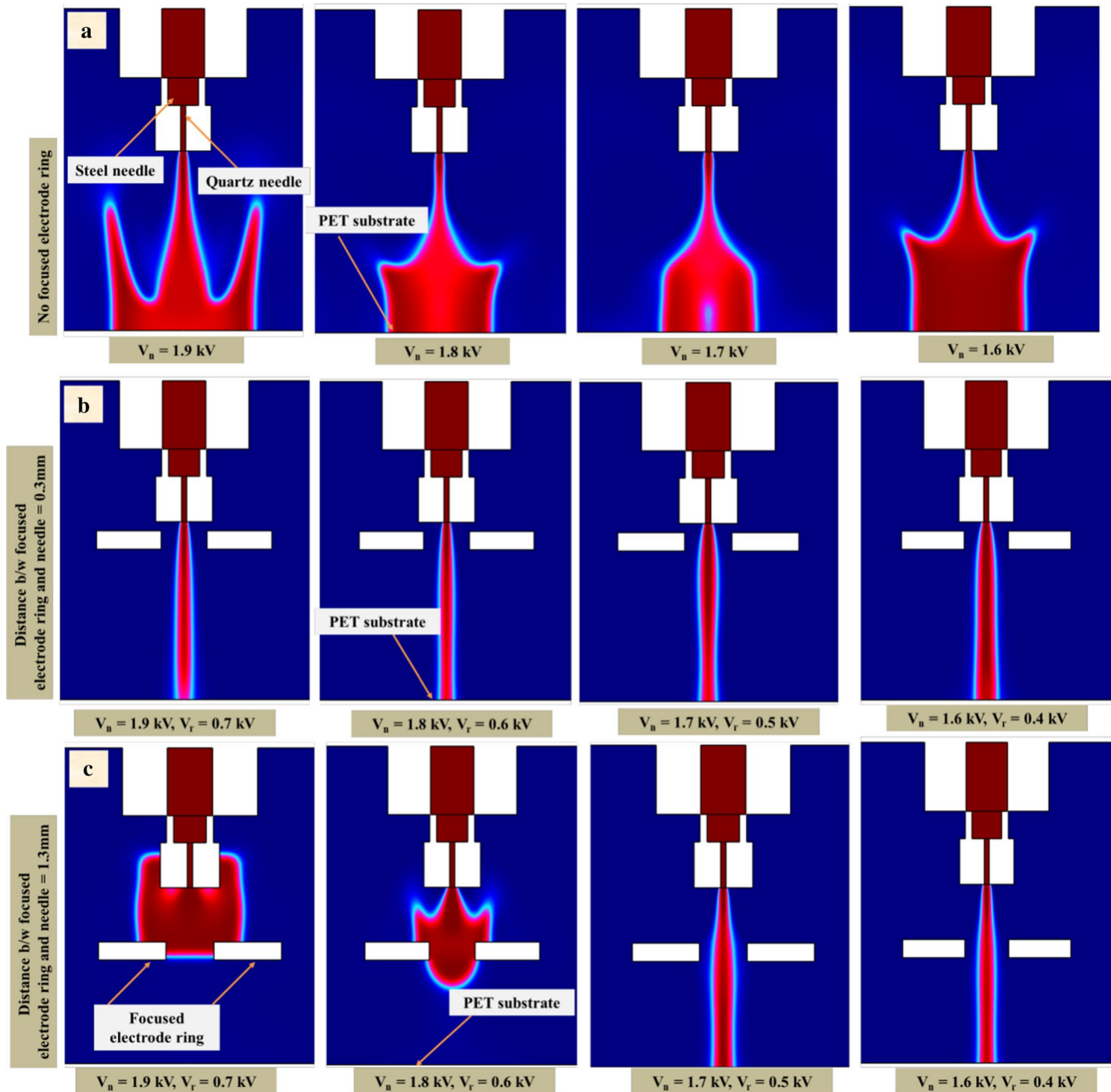

Fig. 7 The (**a**) different specific morphologies of simulated DoD E-Jet without focused electrode ring, and (**b** & **c**) the different specific morphologies of simulated DoD E-Jet using focused electrode ring at different locations keeping all parameters constant

0.7 kV. For flow rate the values vary such as $f = 5.3 \times 10^{-14}$ $m^3\ s^{-1}$ and $5.3 \times 10^{-15}\ m^3\ s^{-1}$. Figure 7a represents simulation morphologies without using of a focused electrode ring by applying dc pulse voltages i.e., $V_n = 1.5$ kV to 1.9 kV at combined needle keeping all other parameters constant. In addition, Fig. 7b and c represent simulation morphologies using a focused electrode ring at different locations applying similar parameters as applied in without focused electrode ring model. The simulation results showed if there is no electrode ring, then the proper DoD E-Jet morphology does not evolve due to exceeding residue charges on the surface of a PET substrate. When the applied voltage was $V_n = 1.7$ kV on combined needle, then cone-jet morphology was thick in shape due to low voltage value which produce weak electric field lines that get away from the needle tip. Further, as the voltage increases at combined needle, the morphology of cone-jet varies in small size, however it does not produce microdripping mode at $V_n = 1.9$ kV.

Successively, a focused electrode ring was placed under the combined needle system at a distance of 0.3 mm and the voltage was applied i.e., $V_n = 1.5$ kV to 1.9 kV at combined needle and $V_r = 0.3$ kV to 0.7 kV at focused electrode ring, respectively. Then, the cone-jet diameter becomes smaller in this case leading to cone-jetting mode. The focused electrode position was changed and distance was maintained 1.3 mm by keeping all parameters constant, but the simulated morphologies showed no specific changes in shape and size of cone-jet. To reduce the distance from combined needle to electrode ring illustrates significant development during a series of simulation experiments. When the focused electrode ring distance was reduced to 0.2 mm, then simulated cone-jet mode transforms into microdripping modes which generate spheroidal shape droplets due to strong effect of applied voltage to focused electrode ring. Although, the applied parameters were used similar to other results obtained from simulation as shown in Fig. 8a. In particular, the simulation results showed in Fig. 8a that droplet breaks up due to joint effect of applied voltage and vectors of residual charges opposes their propagation effect on a PET substrate. Therefore, it can be seen that focused electrode ring impact is able to reproduce precisely the droplet detachment time, which is one of the most important operational tools of phase field method. Subsequently, in another simulation experiment the flow rate value was increased respectively from $f = 5.3 \times 10^{-15}\ m^3\ s^{-1}$ to $6.5 \times 10^{-14}\ m^3\ s^{-1}$. However, it can be seen in Fig. 8b that the droplet diameter is different at high value and returns to discharge of the functional liquid, due to charges repulsion of insulating substrates. The small cone-jet diameter is generated by regulating low flow rate value of $f = 5.3 \times 10^{-15}\ m^3\ s^{-1}$ while keeping all other parameters constant. The E-Jet morphology is transformed into pulsation mode in a short time at the outlet of a combined needle interface to form microdroplets. However, this

has occurred due to effect of weak charge density and the effect of strong electrical forces. It has been experimentally proven during numerical simulation that the joint effect of needle system and focused electrode ring is absolutely relevant to the electric field lines generated by high dc positive pulse voltage. The diameter of the microdroplets is obtained smaller on PET substrate, but the morphology of cone-jet disappears and converts into the microdripping mode due to strong voltage effect of focused electrode ring. The simulation results determine that applied voltage is inversely proportional to the microdroplets size and flow rate is in direct proportion to the droplet size. The phenomenon of cone-jetting shows that it can print stable and high-resolution microdroplets using the DoD E-Jet printing method for the application of MEMS devices by regulating dc positive pulse voltage at a focused electrode ring. Finally, the simulated microdroplets on the PET substrate with magnified images are shown in Fig. 8c at identical simulation time intervals of $t = 0.185$ s (scale bar = 20 μm).

3.2 E-Jet Simulation Verification

3.2.1 Drop-on-Demand E-Jet Printing

DoD E-Jet printing uses only enough functional ink to pattern microdroplets and DoD print heads can create gradients and grey scale effects at effective resolutions of 1200 dpi and higher [35]. Among E-jetting modes, the dripping mode, micro-dripping mode, cone-jet mode and multi-jet modes have been widely observed in experiments. Noticeably, for precision manufacturing, the micro-dripping mode (i.e., pulsation) and steady-state convection mode provide the required controllability of a printing process and high resolution which are used as DoD printing and direct writing, respectively. Micro-dripping mode occurs only when the functional ink flow rate and ink dynamic viscosity are low and applied voltage is high. Therefore, amid many jetting modes of E-Jet printing, the micro-dripping mode (i.e., pulsation mode) and steady-state convection mode provide such a high precision fabrication capability [36].

Figure 9a shows schematic illustration of the experimental apparatus using a focused electrode ring. Figure 9b illustrates the focused electrode ring is used to verify numerical simulation results under the optimized parameters. In order to verify simulation results, a series of experimental investigations were performed on a PET substrate at their various thicknesses to obtain high-resolution microdroplets. The results demonstrate that the actual cone-jet and droplet diameter are inversely proportional to the applied voltage, and the needle to substrate distance and the liquid flow rate are in direct proportion. Similarly, the printing microdroplets size on substrate surface is also consistent with this rule which proves the correctness of model and simulation results. To
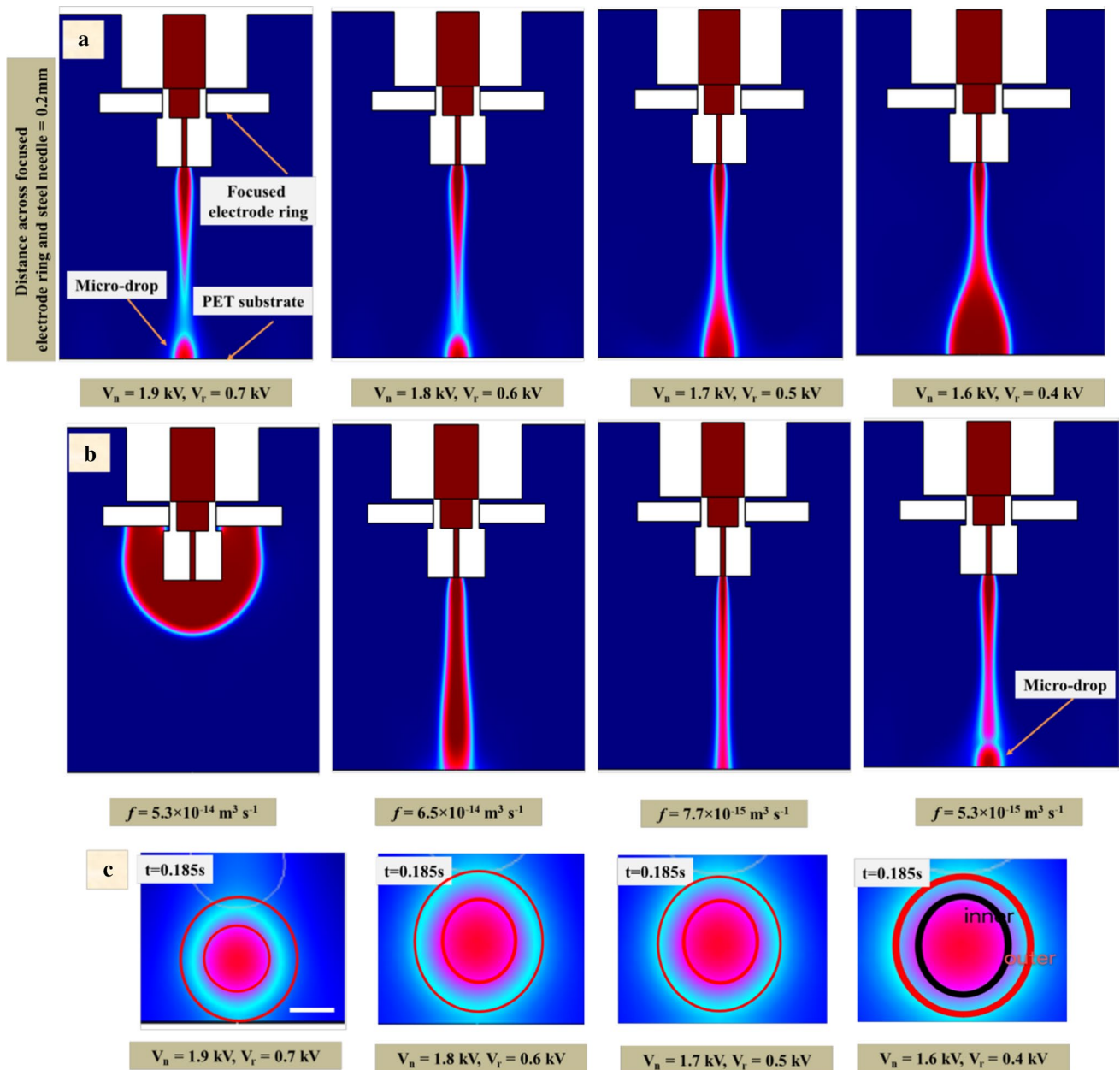
Fig. 8 The (**a**) different specific morphologies of simulated DoD E-Jet at different applied voltages using focused electrode ring, (**b**) the different specific morphologies of simulated DoD E-Jet at dif-ferent flow rates using focused electrode ring and (**c**) The simulated droplets on PET substrate with magnified images, scale bar = 20 μm

obtain small diameter cone-jet morphology and further to generate smaller-sized drops, the applied dc positive pulse voltage must be higher as determined by the numerical simulation. Likewise, as inferred from numerical simulation that the designed focused ring is a highly effective and innovative electrode used in current DoD E-Jet printing. Moreover, it is equally suitable for patterning small size drops on a PET substrate during experimental study. The high dc positive pulse voltage does not produce opposite effect of eddy current on outer surface of focused electrode ring due to

use of insulating retaining holder which adjusts the position of electrode ring. Accordingly, the use of UF3808 as a functional ink in this work was intended to test the simulation parameters by printing stable microdroplets on a PET substrate. Process parameters such as applied voltage, flow rate, focused electrode ring position and needle to substrate distance integrate DoD E-Jet printing with insulating substrates. The experimental setup for droplet generation on PET substrate is shown in Fig. 9c. The microdrops fabricated during simulation and the entire experimental process
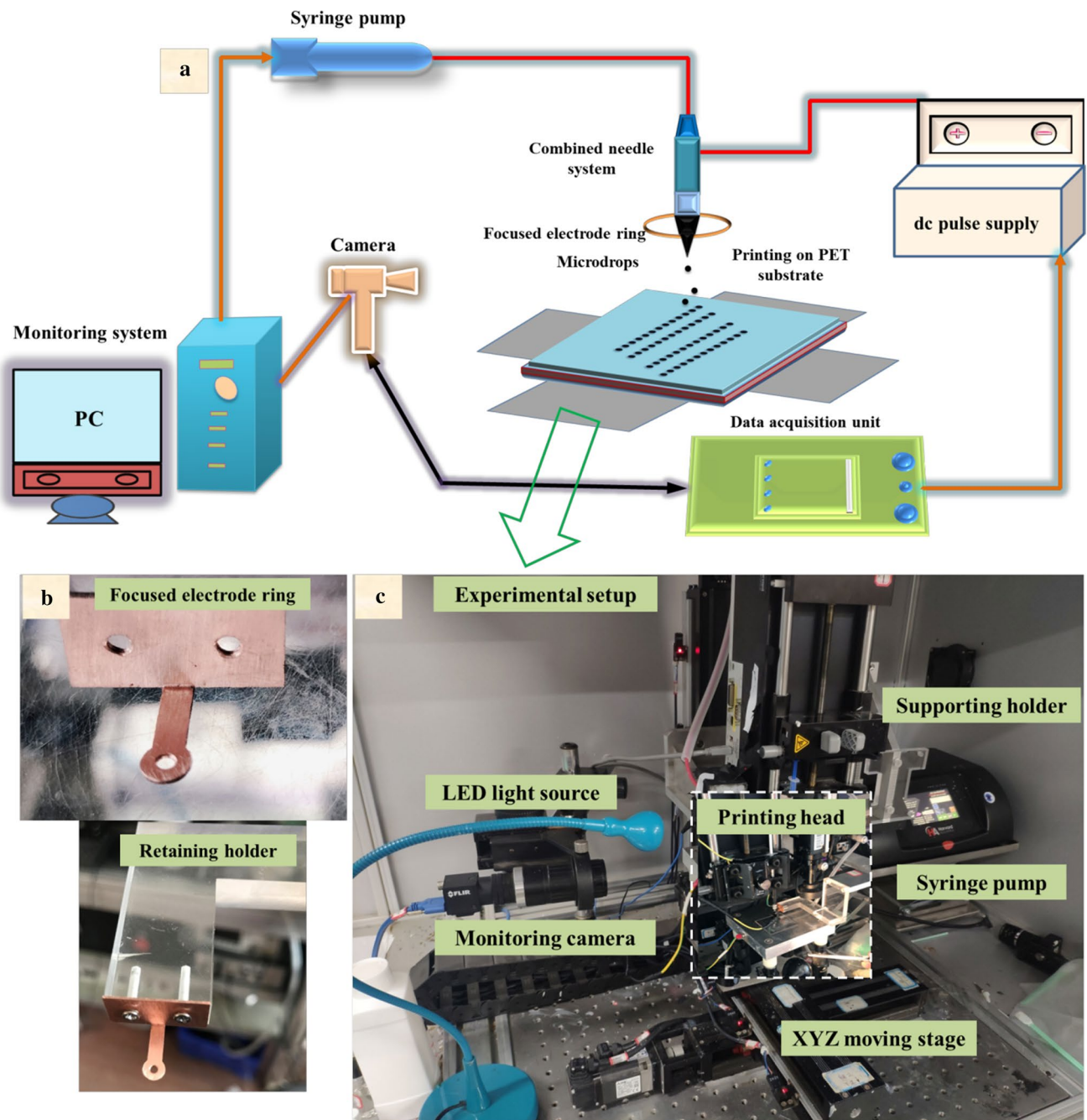
Fig. 9 The (**a**) schematic illustration of the experimental apparatus using a focused electrode ring, (**b**) designed focused electrode ring and (**c**) experimental setup for droplet generation on PET substrate

for the formation of microdroplets on a PET substrate is shown in Fig. 10a and b.

The resolution of DoD E-jet printing can be sub-micrometer. In order to obtain sub-micrometer feature, the needle size should be reduced to sub-micrometer as well. In addition, the needle-substrate distance should be reduced to hundreds of nanometers in order to focus the electric field. However, with the use of coaxial needle the feature size down to 100 nm can be printed [37]. In this method, the electrical shearing force and electrical field induce viscous shearing force and internal pressure that are jointly applied on the inner ink by focusing the inner jet on nanoscale and printing nanoscale structure. This method realizes the printing of nanoscale structures with the use of a one hundred micrometer-sized needle and has the capability to print nanoscale structures on flexible substrate for NEMS devices.
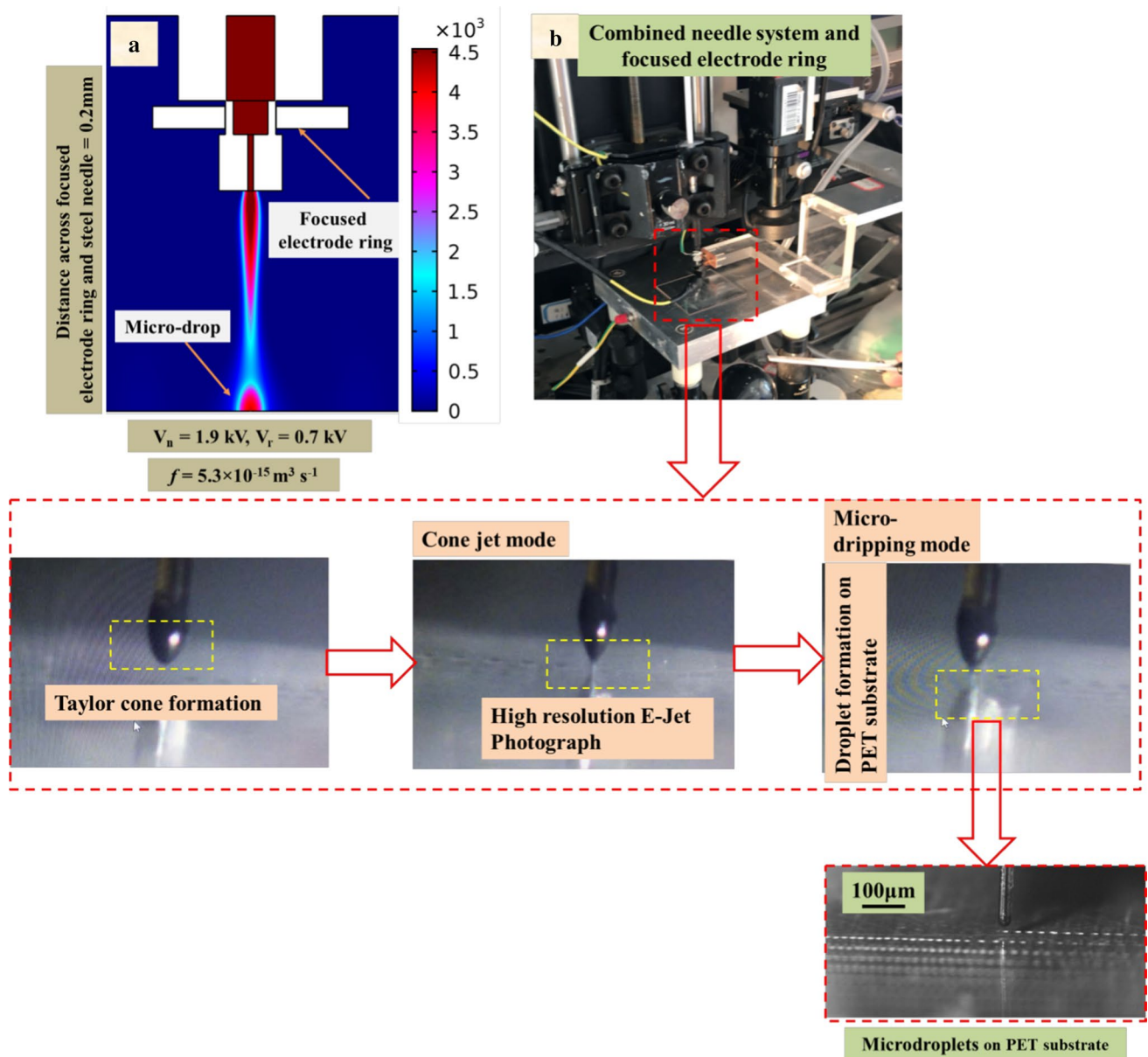
Fig. 10 The (**a**) simulation results for droplet generation on PET substrate and (**b**) complete experimental process for droplet generation on PET substrate

The low value of liquid flow rate and high dc positive pulse voltage ($f = 5.3 \times 10^{-15}$ m³ s⁻¹, $V_n = 1.9$ kV, $V_r = 0.7$ kV) were obtained and used as optimized parameters to print various microstructures by using constant frequency of 100 Hz and duty cycle of 80%. Subsequently, various DoD patterns began to be printed directly on the insulating PET substrate using printing speed 200 mm/s. Furthermore, Fig. 11 illustrates different droplet string structures that are printed on a PET substrate which has widths of 0.5 mm and 0.2 mm respectively. The optimized process parameters are respectively the exact same as those used in numerical simulation. In printing process, the parameters

such as printing trajectory, printing speed, applied voltage, and flow rate are linked and controlled accordingly the simulation results. Figure 11a and b show the "droplets string" patterns printed at room temperature using UF3808 with a viscosity of 450,000 cps. The microstructures are uniform and continuous, and there is no glue line breakage and accumulation in each droplet. The minimum droplet size was measured 3 μm (standard deviation: 1.5 μm) in the printed microstructures, and the aspect ratio is about 0.4. The printing results of microdroplets string prove that the parameters used are perfect for flexible printed electronics in MEMS devices. Furthermore, which increase their stability and
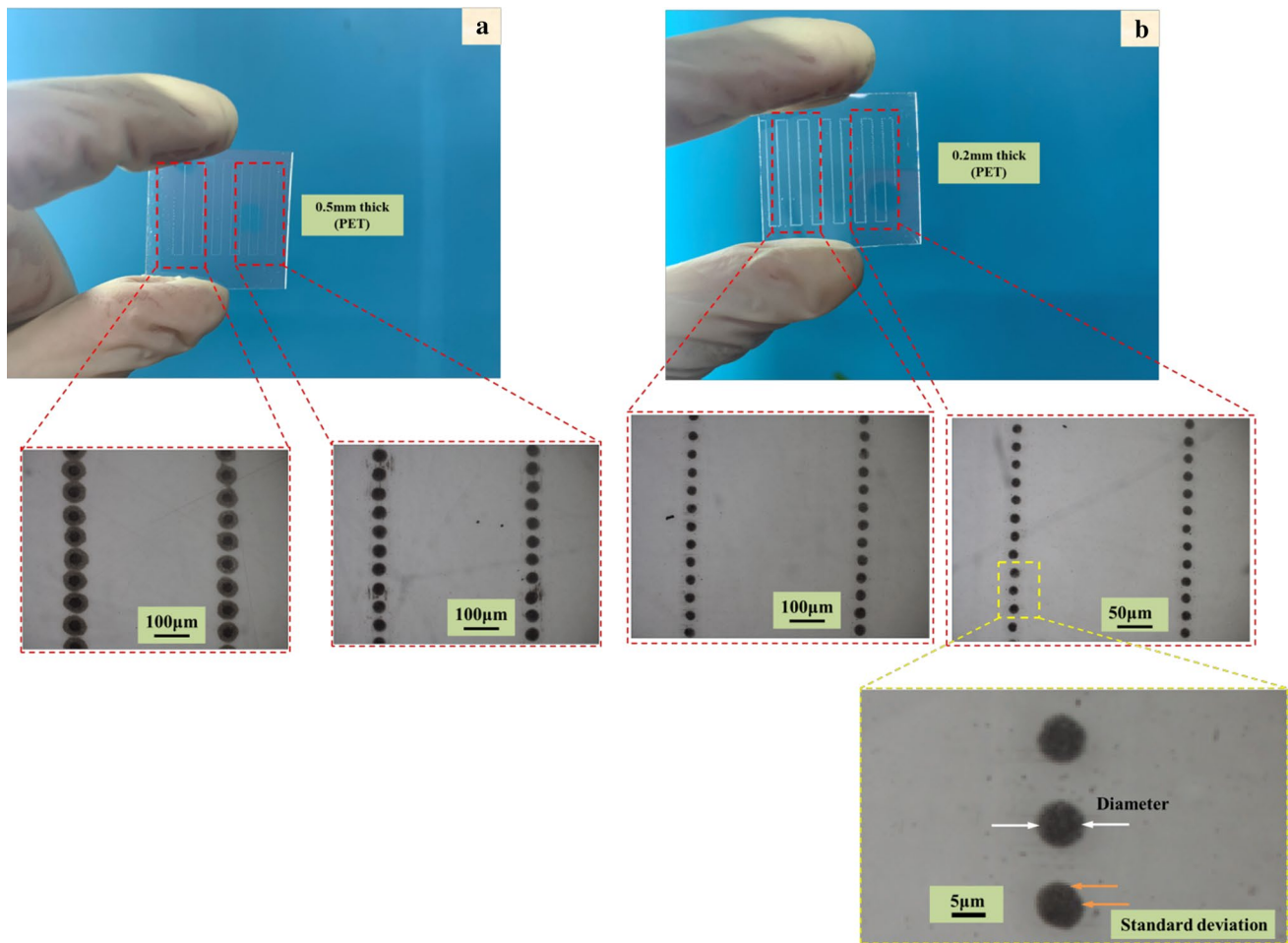
Fig. 11 The strings of DoD E-Jet printing on PET substrates with various widths (**a**) 0.5 mm width and (**b**) SEM images of drops patterned on PET with 0.2 mm width

resolution by using DoD E-Jet printing technique. It was also discovered from the simulation model that capability and versatility of a DoD method for well-adjusted microscale structures on PET substrate is inevitable in future.

Figure 12 displays droplet array on a PET substrate having a width of 0.2 mm. The droplet size was measured 15 μm on PET substrate (thickness = 0.5 mm) which is very small compared to the quartz capillary diameter. Although, the extracted droplets are half to one-third of a diameter of the combined needle, the propagation of the puncture droplet increases its size to 4.5 μm on PET substrate (thickness = 0.2 mm). The performance of thick PET substrate is similar to that of PET which has a width of 0.2 mm, except that the droplet strings on PET having a width of 0.5 mm is a several times larger than those having a width of 0.2 mm. Further, the PET substrate with less width allows the reduction of diffusion in the impact of particles on substrate surface due to its anti-residue charge effect. The magnified views of printed strings after complete evaporation of the solvent are shown in Fig. 12. An optical microscope was

used to capture these high-resolution images. Although, the functional ink particles are not optimally dispersed, nevertheless aggregation is observed. More, the microdroplets retain the desired circular shape by containing minimum size of 46 μm in printed droplet strings as shown in Fig. 11. Because functional ink particles are relatively large in size, the coffee ring effect is not noticeable [38]. This is another advantage of using large size particles in microdroplet i.e., non-nanoscale.

4 Conclusion

The DoD E-Jet printing technology was explored for potential use in MEMS devices, especially for flexible printed circuits. In this work, we present a phase field method to generate a stable cone-jet morphology that can allow the production of micron/nano structures on PET substrates. In particular, the study introduces a distinctive combination of needle and focused electrode ring, which has a significant

Fig. 12 The printed droplets array on PET substrate with magnified images
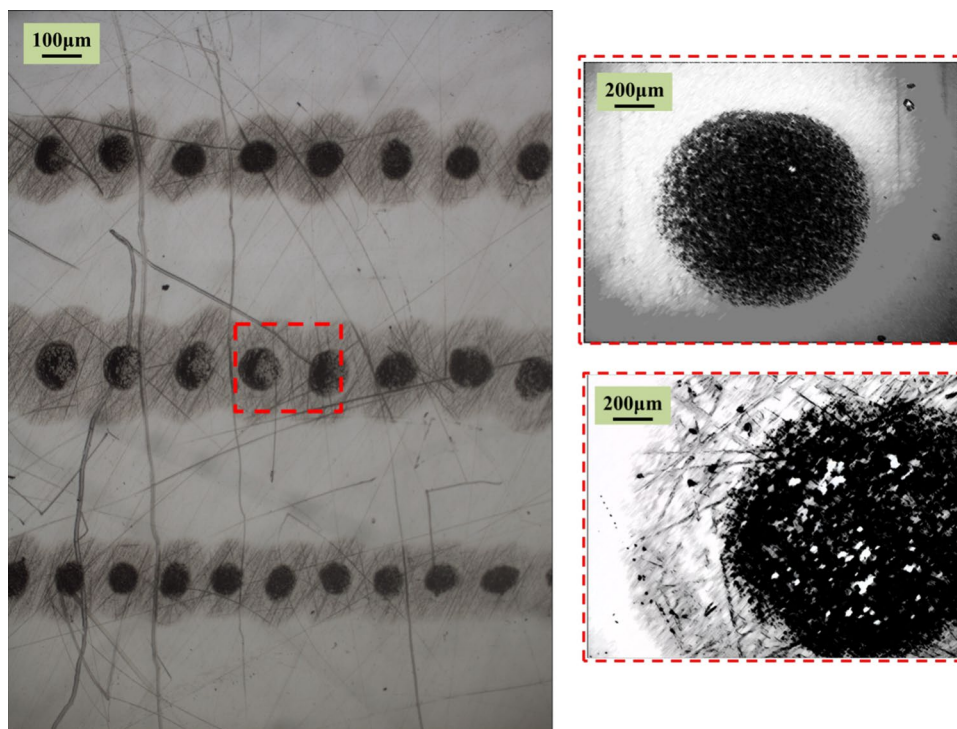
impact on stability and resolution of microdroplets. Firstly, the numerical simulation of cone-jet morphology was performed. A Taylor-Mechler leaky dielectric model was established for Taylor cone generation and effects of each force on the cone-jet were examined. The motion equation, the electric field equation and the interface tracking equation between liquid and air were derived using the Navier–Stokes equation and the Maxwell pressure tensor method. The physical model was transformed into a geometric model and boundary conditions were set. The numerical simulation of DoD E-Jet was performed to analyze the influence of key printing parameters on a cone-jet morphology. Further, the impact of needle and focused electrode ring voltage were studied on the cone-jet profile. The results exhibit that microdroplet diameter is inversely proportional to the dc pulse voltage and directly proportional to the liquid flow rate. To sum up, optimized parameters by simulation were directly used to print arrays of stable droplets on PET substrate using UF 3808 ink during the experimental study. This model gains recognition as a novel, low cost, high speed and environmentally-friendly in manufacturing process. More, this model can provide guidance for optimizing the DoD E-Jet printing process and a quick determination of operation parameters for the desired printing resolution in E-Jet printing for MEMS devices.

Declarations

Conflict of interest The authors declare that they have no competing financial interests.

References

1. Algamili, A. S., Khir, M. H. M., Dennis, J. O., Ahmed, A. Y., Alabsi, S. S., Ba Hashwan, S. S., & Junaid, M. M. (2021). A review of actuation and sensing mechanisms in MEMS-based sensor devices. *Nanoscale Research Letters, 16.* https://doi.org/10.1186/s11671-021-03481-7.
2. Bao, M., & Wang, W. (1996). Future of microelectromechanical systems (MEMS). *Sensors and Actuators, A: Physical, 56*, 135–141. https://doi.org/10.1016/0924-4247(96)01274-5
3. Sahdom, A. S. (2019). Application of micro electro-mechanical sensors (MEMS) devices with wifi connectivity and cloud data solution for industrial noise and vibration measurements. *Journal of Physics: Conference Series, 1262.* https://doi.org/10.1088/1742-6596/1262/1/012025.
4. Abbas, Z., Wang, D., Du, Z., Qian, J., Zhao, K., & Du, Z. (2020). Numerical simulation of electrohydrodynamic jet and printing micro- structures on flexible substrate. *Microsystem Technologies, 1.* https://doi.org/10.1007/s00542-020-05068-1.
5. Chan, M. L., Yoxall, B., Park, H., Kang, Z., Izyumin, I., Chou, J., Megens, M. M., Wu, M. C., Boser, B. E., & Horsley, D. A. (2012). Design and characterization of MEMS micromotor supported on low friction liquid bearing. *Sensors and Actuators, A: Physical, 177*, 1–9. https://doi.org/10.1016/j.sna.2011.08.003

6. Lee, B., Seok, S., & Chun, K. (2003). A study on wafer level vacuum packaging for MEMS devices. *Journal of Micromechanics and Microengineering, 13*, 663–669. https://doi.org/10.1088/0960-1317/13/5/318

7. Park, Y., Oh, O., & Noh, M. D. (2015). Ejection feasibility of high viscosity fluid with magnetostrictive inkjet printhead,*16*, 1369–1374. https://doi.org/10.1007/s12541-015-0180-4.

8. Abbas, Z., Wang, D., Du, Z., Zhao, K., Du, Z., & Lu, L. (2021). Microelectronic Engineering Numerical simulation of stable electrohydrodynamic cone-jet formation and printing on flexible substrate. *Microelectronic Engineering, 237*, 111496. https://doi.org/10.1016/j.mee.2020.111496

9. Riheen, M. A., Saha, T. K., & Sekhar, P. K. (2019). Inkjet printing on PET substrate. *Journal of the Electrochemical Society, 166*, B3036–B3069. https://doi.org/10.1149/2.0091909jes

10. Hebner, T. R., Wu, C. C., Marcy, D., Lu, M. H., & Sturm, J. C. (1998). Ink-jet printing of doped polymers for organic light emitting devices. *Applied Physics Letters, 72*, 519–521. https://doi.org/10.1063/1.120807

11. Sirringhaus, H., Kawase, T., Friend, R. H., Shimoda, T., Inbasekaran, M., Wu, W., & Woo, E. P. (2000). High-resolution inkjet printing of all-polymer transistor circuits. *Science, 290*, 2123–2126. https://doi.org/10.1126/science.290.5499.2123

12. Choi, J., Lee, S., Kim, Y. J., Son, S. U., & An, K. C. (2012). High aspect ratio EHD printing with high viscosity ink ejection. In *Technical Proceedings of the 2012 NSTI Nanotechnology Conference and Expo, NSTI-Nanotech 2012* (pp. 267–270).

13. Choi, J., Kim, Y. J., Lee, S., Son, S. U., Ko, H. S., Nguyen, V. D., & Byun, D. (2008). Drop-on-demand printing of conductive ink by electrostatic field induced inkjet head. *Applied Physics Letters, 93*, 87–90. https://doi.org/10.1063/1.3020719

14. Wei, C., Qin, H., Chiu, C., Lee, Y., & Dong, J. (2015). Drop-on-demand E-jet printing of continuous interconnects with AC-pulse modulation on highly insulating substrates. *Journal of Manufacturing Systems, 37*, 505–510. https://doi.org/10.1016/j.jmsy.2014.07.005

15. Wang, D., Abbas, Z., Lu, L., Zhao, X., Xu, P., Zhao, K., Yin, P., & Liang, J. (2022). Numerical modeling and analysis of coaxial electrohydro dynamic jet printing. *Scientific Reports, 12*, 1–17. https://doi.org/10.1038/s41598-022-05596-y

16. Yuan, S., Si, T., Liu, Z., & Xu, R. X. (2014). Microfabrication of curcumin-loaded microparticles using coaxial electrohydrodynamic atomization. *Reporters, Markers, Dyes, Nanoparticles, and Molecular Probes for Biomedical Applications VI, 8956*, 895618. https://doi.org/10.1117/12.2041070

17. Kim, J., Oh, H., & Kim, S. S. (2008). Electrohydrodynamic drop-on-demand patterning in pulsed cone-jet mode at various frequencies,*39*, 819–825. https://doi.org/10.1016/j.jaerosci.2008.05.001.

18. Emission, A., Hakiai, K., Ishida, Y., Asano, T., Driving, I., Ishida, Y., Sogabe, K., Electrospray, D., Ishida, Y., Sogabe, K., Lee, S., Kim, J., Driving, I., & Emission, A. (2005). Electrostatic droplet ejection using planar needle inkjet head. https://doi.org/10.1143/JJAP.44.5781.

19. Rahman, K., Ali, K., Muhammad, N. M., Hyun, M. T., & Choi, K. H. (2013). Fine resolution drop-on-demand electrohydrodynamic patterning of conductive silver tracks on glass substrate. *Applied Physics A: Materials Science and Processing, 111*, 593–600. https://doi.org/10.1007/s00339-012-7267-x

20. Li, J., & Zhang, P. (2009). Formation and droplet size of EHD drippings induced by superimposing an electric pulse to background voltage. *Journal of Electrostatics, 67*, 562–567. https://doi.org/10.1016/j.elstat.2008.11.007

21. Rahman, K., Ko, J., Khan, S., Kim, D., & Choi, K. (2010). Simulation of droplet generation through electrostatic forces † *24*, 307–310.

22. Rahman, K., Khan, A., Nam, N. M., Choi, K. H., & Kim, D. (2011). Study of drop-on-demand printing through multistep pulse voltage,*12*, 663–669. https://doi.org/10.1007/s12541-011-0086-8.

23. Wang, C., & Smith, K. A. (2011). Numerical simulation of cone-jet formation in electrohydrodynamic atomization,*57*, 57–78. https://doi.org/10.1002/aic.

24. Schnitzer, O., & Yariv, E. (2015). The Taylor-Melcher leaky dielectric model as a macroscale electrokinetic description. *Journal of Fluid Mechanics, 773*, 1–33. https://doi.org/10.1017/jfm.2015.242

25. Saville, D. A. (1997). Electrohydrodynamics: The Taylor-Melcher leaky dielectric model. *Annual Review of Fluid Mechanics, 29*, 27–64. https://doi.org/10.1146/annurev.fluid.29.1.27

26. Jacqmin, D. (1999). Calculation of two-phase Navier-Stokes flows using phase-field modeling. *Journal of Computational Physics, 155*, 96–127. https://doi.org/10.1006/jcph.1999.6332

27. Herrada, M. A., Vega, E. J., Montanero, J. M., & Popinet, S. (2021). Numerical simulation of electrospray in the cone-jet mode,*026305*, 1–8. https://doi.org/10.1103/PhysRevE.86.026305.

28. Boyer, F., Lapuerta, C., Minjeaud, S., Piar, B., & Quintard, M. (2010). Cahn-Hilliard/Navier-Stokes model for the simulation of three-phase flows. *Transport in Porous Media, 82*, 463–483. https://doi.org/10.1007/s11242-009-9408-z

29. Sheehy, P., & Owkes, M. (2017). Numerical study of electric Reynolds number on electrohydrodynamic (EHD) assisted atomization, *27*, 645–664.

30. Kim, S. Y., Kim, Y., Park, J., & Hwang, J. (2010). Design and evaluation of single nozzle with a non-conductive tip for reducing applied voltage and pattern width in electrohydrodynamic jet printing (EHDP). *Journal of Micromechanics and Microengineering, 20* (2010). https://doi.org/10.1088/0960-1317/20/5/055009.

31. Zhao, X., Wang, D., Lin, Y., Sun, Y., Ren, T., Liang, J., & Madou, M. (2019). Numerical simulation of coaxial electrohydrodynamic jet and printing nanoscale structures. *Microsystem Technologies*. https://doi.org/10.1007/s00542-019-04499-9

32. Lastow, O., & Balachandran, W. (2006). Numerical simulation of electrohydrodynamic (EHD) atomization. *Journal of Electrostatics, 64*, 850–859. https://doi.org/10.1016/j.elstat.2006.02.006

33. Zhao, X., Wang, D., Lin, Y., Sun, Y., Ren, T., Liang, J., & Madou, M. (2019). Numerical simulation of coaxial electrohydrodynamic jet and printing nanoscale structures. *Microsystem Technologies, 25*, 4651–4661. https://doi.org/10.1007/s00542-019-04499-9

34. Yin, Z., Huang, Y. A., Duan, Y., & Zhang, H. (2017). Electrohydrodynamic direct-writing for flexible electronic manufacturing. https://doi.org/10.1007/9789811047596.

35. Rahman, T. T., Arman, M. S., Perez, V., Xu, B., & Li, J. (2021). Analysis of the operating conditions of pulse electric field–assisted EHD for sodium alginate printing using design of experiment approach. *International Journal of Advanced Manufacturing Technology, 115*, 2037–2047. https://doi.org/10.1007/s00170-021-07042-1.

36. Han, Y., & Dong, J. (2018). Electrohydrodynamic printing for advanced micro/nanomanufacturing: Current progresses, opportunities, and challenges. *Journal of Micro and Nano-Manufacturing, 6*. https://doi.org/10.1115/1.4041934.

37. Wang, D., Zhao, X., Lin, Y., Liang, J., Ren, T., Liu, Z., & Li, J. (2018). Nanoscale coaxial focused electrohydrodynamic jet printing. *Nanoscale, 10*, 9867–9879. https://doi.org/10.1039/c8nr01001c

38. Kang, D. K., Lee, M. W., Kim, H. Y., James, S. C., & Yoon, S. S. (2011). Electrohydrodynamic pulsed-inkjet characteristics of various inks containing aluminum particles. *Journal of Aerosol Science, 42*, 621–630. https://doi.org/10.1016/j.jaerosci.2011.06.009

Zeshan Abbas accomplished his M.Eng degree at Mehran University of Engineering and Technology Jamshoro, Pakistan in 2017. Since 2018, he is studying a Ph.D in Key Laboratory for Micro/Nano Technology and System of Liaoning Province, Dalian University of Technology, China. He has been studying Micro-nano devices and simulation & modeling of electrohydrodynamic jet printing on flexible polymer substrates.

Dazhi Wang is a Professor in the School of Mechanical Engineering, Dalian University of Technology, China. He received his M.Eng and Ph.D degree in materials science from Queen Mary University of London in 2003 and 2006. He worked in Cranfield University as a research officer from 2006–2008. His current research interests are: (1) nanoprinting and nanodevices, (2) high performance piezoelectric microsystems, (3) design and manufacture of multi-parameters transducer for complex working conditions.

Liangkun Lu completed his M.Eng degree at Guilin University of electronic science and technology in China in 2019. Now, he is studying Ph.D in Key Laboratory for Micro/Nano Technology and System of Liaoning Province, Dalian University of Technology, China. He has been studying micro-nano printing, Electro-Hydrodynamics.

Zhaoliang Du completed his graduation from Henan University of science and technology in 2019. Now he is studying M.Eng in Key Laboratory for Micro/Nano Technology and System of Liaoning Province, Dalian University of Technology, China. The latest research field is the research and design of EFI printing control program.

Xiangyu Zhao completed his graduation from Zhengzhou University in 2018. Now he is studying M.Eng in Key Laboratory for Micro/Nano Technology and System of Liaoning Province, Dalian University of Technology, China. The latest research is the printing and testing of nano-beams.

Kuipeng Zhao completed his M.Eng degree at Shaanxi University of Science and Technology in 2013. Now he is studying Ph.D in Key Laboratory for Micro/Nano Technology and System of Liaoning Province, Dalian University of Technology, China. He has been studying micro-nano printing, fabrication of microsensor and microactuator.

Meng Si completed her graduation from Yanshan University in 2019. Now she is studying M.Eng in school of Opto-electronic Engineering and Instrument Science, Dalian University of Technology, China. The latest research field is the research and design of electrofluid jet printing technology.

Penghe Yin is an engineer at Dalian University of Technology. He received a bachelor degree from Dalian University of Technology in 2006 and a master degree from Shanghai Jiaotong University in 2009. Since 2011, he has been an engineer in the Key Laboratory for Micro/Nano Technology and System of Liaoning Province.

Junsheng Liang is a researcher/doctor supervisor obtaining bachelor's degree from Hefei University of Technology in 1995 and master's degree from Guilin University of electronic science and technology in 2003, and doctor's degree from Dalian university of technology in 2007. He is focusing on micro-nano manufacturing and MEMS devices.

Xi Zhang is an engineer at Dalian University of Technology. She received a bachelor's degree from Tianjin University in 2005 and a master's degree in engineering from Beijing University of Chemical Technology in 2008. Since 2010, she has been an engineer in the Key Laboratory for Micro/Nano Technology and System of Liaoning Province.

Yan Cui is a Professor in the School of Mechanical Engineering, Dalian University of Technology, China. She received bachelor and master degree from Dalian University of Technology in 1989 and 1999, and the second master degree in Sensor Systems Technology from Karlsruhe University of Applied Sciences, Germany in 2003. Her current research interests are microelectromechanical engineering, precision instruments and machinery, test and measurement technology and instruments.